

Synthesis and characterisation of FeTiO₃ perovskite nanomaterials for electrochemical energy storage application

Satturappa Ravisekaran Srither¹ ✉, Nattanmai Raman Dhineshabu²

¹Department of Physics, South University of Science and Technology, Shenzhen, People's Republic of China

²Department of Materials Engineering, Indian Institute of Science, Bangalore, India

✉ E-mail: srither10@gmail.com

Published in Micro & Nano Letters; Received on 23rd October 2018; Revised on 11th December 2018; Accepted on 3rd January 2019

In this study, ilmenite [iron titanate (FeTiO₃)] perovskite nanoparticles were synthesised by wet chemical method and sintered at two temperatures, namely 350°C (FT350) and 500°C (FT500). The phase structure, crystallinity, microstructure, particle size, and purity of the sintered samples were extensively studied. Electrochemical measurements such as cyclic voltammetric studies, electrochemical impedance spectroscopy (EIS), and discharge measurements were carried out. The results of the cyclic voltammetric studies showed that sample prepared at 500°C delivers high specific capacitance (42 F g⁻¹), which is significantly greater as compared to that of 350°C sample. Moreover, the results of the EIS study show that 500°C delivers better capacitance than 350°C. The FeTiO₃ samples sintered at 350 and 500°C used as cathodes in a novel Mg/FeTiO₃ cell delivered a discharge capacity of 129 and 90 mA h g⁻¹, respectively. According to the study's data, for the first time it has confirmed that FeTiO₃ is suitable for using it as a cathode material in Mg/FeTiO₃ primary cell. The discharge capacity of 500°C was found to be 70% higher when compared to 350°C. Thus, the proposed results show that the electrochemical behaviour of the sintered sample 500°C is superior to that of 350°C.

1. Introduction: Metal oxide composites have a vital role in many technological domains, such as catalysis, sensors, magnetic storage, biomedical applications, and energy storage devices [1]. Recent advances in the field of nanomaterials suggest that the unique characteristics of metal oxides may be used in energy storage applications. For example, metal oxide nanocomposites have been prepared and used in the fabrication of solar cells [2], batteries [3], and supercapacitors [4]; however, their utility has not been extensively investigated in the field of energy storage and conversion.

A supercapacitor or electrochemical capacitor is an important energy storage device, capable of providing high power density storage [5]. Supercapacitors are widely used in various applications such as large-scale industrial equipment, memory backup devices, hybrid electric vehicles, renewable energy power plants, and devices providing uninterrupted power supplies in computers [6]. In the past decade, materials such as transition metal oxides (ruthenium oxide) and conducting polymers have been used in the fabrication of supercapacitors [7]. Presently, metal oxides and their nanocomposites such as manganese oxide (MnO₂), iron oxide (Fe₃O₄), iridium oxide (IrO₂), cobalt oxide (Co₃O₄), nickel oxide (NiO), tin oxide (SnO₂), ferrites, and perovskites have been usefully applied in the fabrication of supercapacitors because of their superior material properties [8].

Iron oxide-based materials are extensively used as anodes in batteries [9] and fuel cells [10], as cathodes/anodes in supercapacitors [11], as membranes in sensors [12], and as magnetic materials in memory storage devices [13]. However, iron oxide-based materials when used as cathodes in energy storage devices show poor performance and energy capacity than manganese oxide-based materials used as cathodes [14].

Ilmenite [iron titanate (FeTiO₃)] nanoparticles are one of the potential materials that can be used in energy storage applications and in their native form, the production of TiO₂. Nanostructured FeTiO₃ shows interesting properties and has been used as a photocatalyst with enriched photocatalytic activity [15]. It also shows unique magnetic [16] and semiconducting properties, with a bandgap of 2.54–2.58 eV [17, 18]. Previously, the synthesis of FeTiO₃ nanoparticles was reportedly carried out using chemical

and citrate gel methods [19]; hydrothermal [20], sol–gel [21], liquid mix, and H₂/H₂O₂ reduction processes [22]; solid-state reaction [23]; and ball milling [16] methods. As we seen from this Letter, it has promising electrochemical properties relevant to the area of energy storage. Nanostructured FeTiO₃ is a fascinating example of ternary oxides incorporating two types of multivalent metal cations since such oxides may exhibit novel mechanisms of charge storage leading to higher capacitances and wide potential windows. To the best of our knowledge, first time we introduce FeTiO₃ for using as an active cathode material with Mg anode in magnesium based primary cell.

In this study, FeTiO₃ nanoparticles were synthesised and sintered at two temperatures (350 and 500°C), and their specific capacitance values were determined in Na₂SO₄ electrolyte using cyclic voltammetric measurements. The capacitance (42 F g⁻¹) of FeTiO₃ nanoparticles synthesised at 500°C was found to be higher than that of FeTiO₃ nanoparticles (23 F g⁻¹) synthesised at 350°C, and still larger than that of iron oxide nanoparticles (25 F g⁻¹) [8]. In addition to capacitance measurements, the physical and chemical properties of the two synthesised FeTiO₃ nanoparticle samples were also investigated using X-ray diffractometer (XRD), Fourier transform infrared (FTIR) spectroscopy, scanning electron microscopy (SEM), and energy-dispersive X-ray spectrometer (EDAX). These measurements were further augmented by electrical discharge measurement and electrochemical impedance spectroscopy (EIS) to further distinguish any differences between the two sintered samples.

2. Materials and methods: All chemical reagents used in the investigation were purchased from Sigma-Aldrich, India and were used without any further purification. To synthesise the FeTiO₃ nanoparticles, we initially dissolved 4.04 g (0.1 M) ferric nitrate (Fe(NO₃)₃·9H₂O) in 100 ml double-distilled water and stirred vigorously. This aqueous solution was used to dissolve 0.5 ml (0.1 M) titanium dioxide and stirred for 2 h, after which 10 ml ethanol was added under constant stirring condition. After a few minutes, 15 ml acetylacetone was further added to the solution. The mixture was again stirred continuously for another 2 h until a deep brown precipitate was formed. This solution was then washed first in

ethanol and then in deionised water. The prepared colloidal solution was dried in a hot-air oven at 100°C for 24 h. The dried FeTiO₃ nanoparticle powder was sintered at 350°C (sample FT350) and 500°C (sample FT500) in a muffle furnace for 1 h at atmospheric pressure.

3. Characterisation: The structural features of the two sintered samples in pellet form, prepared at 350 and 500°C, were experimentally determined using an XRD (X'Pert PRO; PANalytical, Almelo, the Netherlands). The XRD patterns were obtained using CuK α as a radiation source ($\lambda = 1.5405$ Å) operated under a constant current of 30 mA at 40 kV and with a diffraction angle (2θ) scan range of 10°–80°.

To analyse the functional groups of FeTiO₃ nanoparticles, we mixed a spectral-grade KBr powder at a weight ratio of 1:100 mg with FeTiO₃ nanoparticle powder in an agate mortar, and these powders were pressed into a pellet with a diameter of 13 mm and thickness of 0.5 mm. The infrared absorption spectra of the FeTiO₃ nanoparticle powder composite pellet was obtained using an FTIR spectroscopy (Spectrum 100; PerkinElmer, USA, operated at room temperature) over the wave number range of 4000–400 cm^{−1}. The morphology and composition of the prepared samples (FT350 and FT500) were examined using SEM (JSM-6390LV; JEOL, Japan) and EDAX (JED-2300; JEOL). In addition, the electrochemical discharge measurements, cyclic voltammetry studies, and electrical impedance studies were carried out using PGSTAT302N (Metrohm Autolab, Utrecht, the Netherlands).

4. Results and discussion: Fig. 1 shows the XRD pattern measured for FT350 nanoparticle powder, calcinated at 350°C. A distinct absence of any diffraction peak in the spectrum is indicative of its amorphous nature. In contrast, sample FT500, which was calcinated at 500°C, shows well-defined diffraction peaks at 26.53°, 28.64°, 37.4°, and 57° corresponding to the crystal planes (111), (208), (131), and (060), respectively, and hence is considered to be representative of an orthorhombic crystal structure (JCPDS Card No. 76-2372). The average size of the crystal structure of FT500 sample was ~36 nm, determined using the Scherrer equation [21].

In addition to the XRD measurements, the two samples were subjected to FTIR measurements, as shown in Fig. 2. The plot of the spectral response shows that both the samples exhibit a characteristic absorbance response at 1627 cm^{−1}, which is considered to be due to vibrational stretching of hydroxyl groups. Furthermore, the absorbance band in the wavenumber region of 1600–1300 cm^{−1} for FT350 and FT500 samples is attributed to Fe–O–Fe vibrational mode, whereas the sharp absorbance

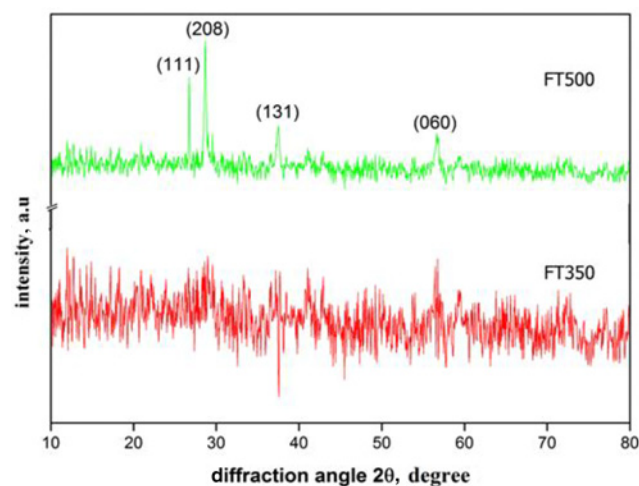


Fig. 1 X-ray diffraction pattern of FT350 and FT500 samples

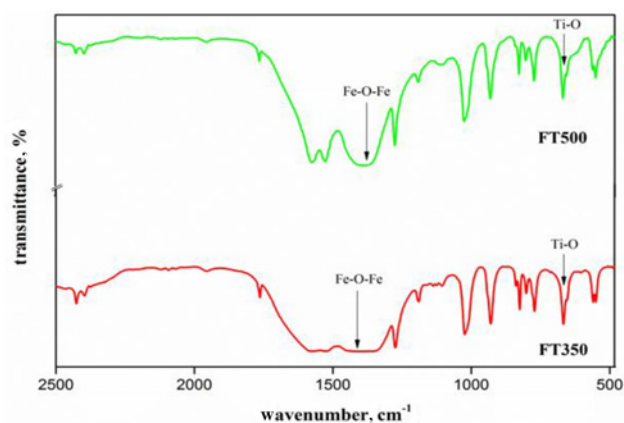


Fig. 2 FTIR spectra of FT350 and FT500 samples

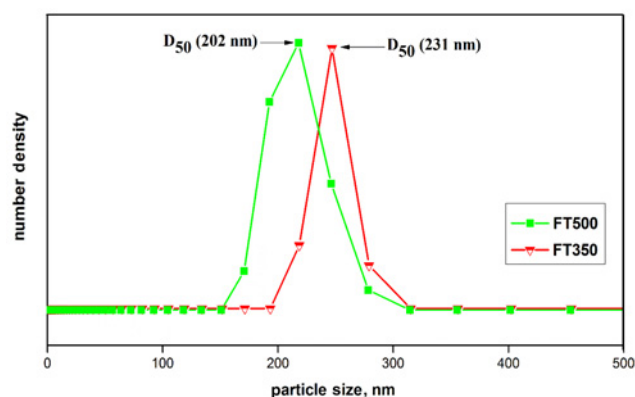


Fig. 3 Particle size distribution of FT350 and FT500 samples

band located in the region of 680–500 cm^{−1} corresponds to the vibrational stretching mode of Ti–Ti.

The plot in Fig. 3 shows particle size distribution of FT350 and FT500 samples, which reveals that the average particle size of FT350 and FT500 samples are 231 and 202 nm, respectively. The difference in the average particle size is attributed to the amorphous nature of FT350, which has greater degree of particle agglomeration, whereas, FT500 sample shows a greater degree of crystallinity with reduced particle dimension due to the higher sintering temperatures used in the production process. The surface morphology and corresponding elemental analyses of FT350 and FT500 samples are shown in Figs. 4a(i, ii) and b(i, ii), respectively. It is apparent from Fig. 4a(i) that FT350 shows greater agglomeration of particles, giving rise to a non-uniform surface morphology. In contrast, FT500 sample shows a more uniform surface morphology with a greater degree of long-range order, with nanosheet structure. The EDAX pattern of the prepared samples FT350 and FT500 indicate the presence of elements Fe, Ti, and O which confirms the sample purity is 100%.

Both the heat-treated FeTiO₃ nanoparticle samples were used in the fabrication of supercapacitor electrodes and their electrochemical performances were investigated using cyclic voltammogram (CV) when immersed in 0.1 M Na₂SO₄ electrolyte. The electrochemical measurements were carried out using PGSTAT302N (Metrohm Autolab, the Netherlands) electrochemistry workstation using a three-electrode electrochemical configuration in which a platinum disk (6 mm in diameter) was used as the working electrode, a platinum foil (1 cm²) as the counter electrode, and a saturated calomel electrode (SCE) as the reference electrode. The working electrode was prepared by mixing 70 wt% sample material, 20 wt% Vulcan carbon (XC-72) as a

conductive material, and 10 wt% polyvinylidene difluoride as a binder [16].

A small amount of *N*-methyl-2-pyrrolidone solvent was added to form a homogeneous mixture for the working electrode.

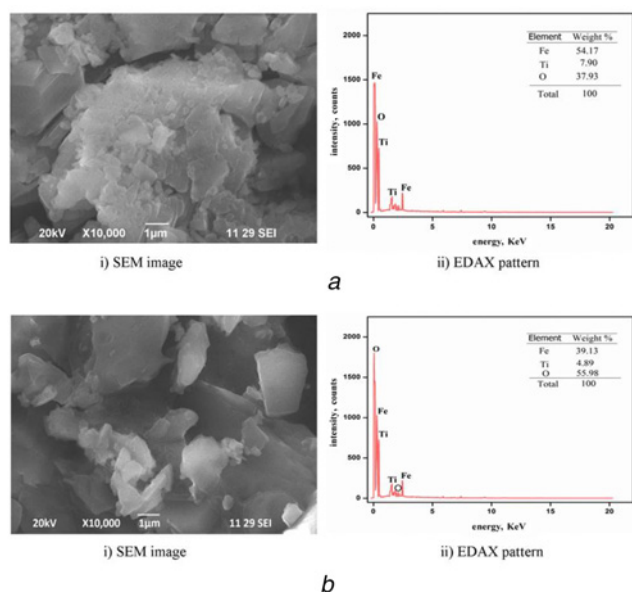


Fig. 4 Microscopic SEM images of FT350 and FT500 samples
a FT350, (i) SEM350, (ii) EDAX pattern
b FT500, (i) SEM350, (ii) EDAX pattern

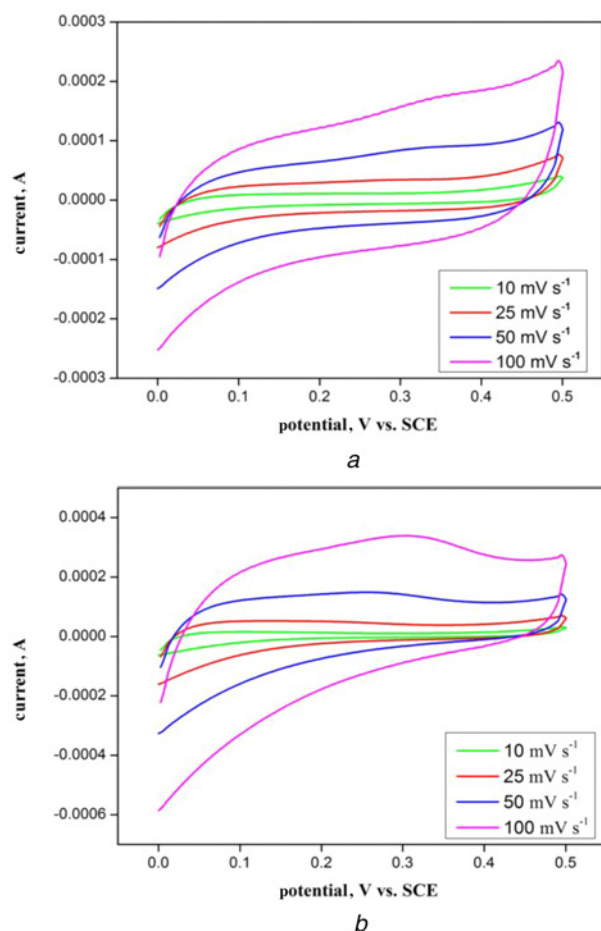


Fig. 5 Cyclic voltammetry studies of FT350 and FT500 samples
a FT350
b FT500

Figs. 5a and b present the CV curves of the FT350 and FT500 samples, at different scan rates, ranging from 10 to 100 mV s^{-1} between 0 and 0.5 V versus SCE. Figs. 5a and b show that the CV curves do not exhibit a redox peak, indicating that the electrodes were charged and discharged at a constant rate over the complete voltammetric cycle. However, the CV plots of FT500 sample show a much-improved capacitive response than those of FT350 sample. Furthermore, the CV response characteristics of FT500 sample are close to that of an ideal rectangular response, expected of the ideal capacitive electrode. The specific capacitances of FT350 sample were calculated as 20, 21, 23, and 22 F g^{-1} at a scan rate of 10, 25, 50, and 100 mV s^{-1} , respectively. Meanwhile, the specific capacitances of FT500 sample are determined to be 23, 31, 40, and 42 F g^{-1} at the respective scan rates of 10, 25, 50, and 100 mV s^{-1} . Thus, on the basis of the above CV data, we can conclude that the capacitance of FT500 sample is sufficiently larger than that of FT350 sample.

The EIS was used to further investigate the characteristic differences between the two samples. Fig. 6 shows the EIS data for the heat-treated sample electrodes FT350 and FT500 measured over the frequency range 0.1–105 Hz in 0.1 M Na_2SO_4 electrolyte solutions. The impedance spectra of FT350 and FT500 samples shown in Fig. 6 exhibit similar characteristics. The linear nature of the complex impedance in the low-frequency region is typical of a diffusion-limited electrochemical process and is represented as the Warburg impedance, whereas the arched response in the high-frequency region is due to the finite resistance of the bulk electrolyte and the electrode interface capacitance. A lumped equivalent circuit that models the observed frequency-dependent impedance characteristics of the two samples is shown in Fig. 6 together with the respective extracted lumped circuit element values. The impedance data show that the extracted charge transfer resistance (R_{ct}) of FT350 sample electrode is higher than that of FT500 electrode due to the larger particle size and greater particle agglomeration of FT350 electrode compared to the smaller particle size and crystallinity of FT500 electrode. Furthermore, the charge storage capacity of FT500 electrode is superior to that of FT350 sample electrode. This finding is in accordance with the result of the cyclic voltammetric test [24].

The discharge transients of the Mg/FeTiO₃ cell for the respective FT350 and FT500 samples are shown in Fig. 7. The fabricated Mg/FeTiO₃ cell was analysed using a galvanostatic constant current of 5 mA discharge with a cutoff voltage of 0.2 V. The initial open-circuit voltages obtained for FT350 and FT500 cells are 1.26 and 1.4 V, respectively. The discharge characteristics of FT350 and FT500 cells, as shown in Fig. 7, are distinctly different.

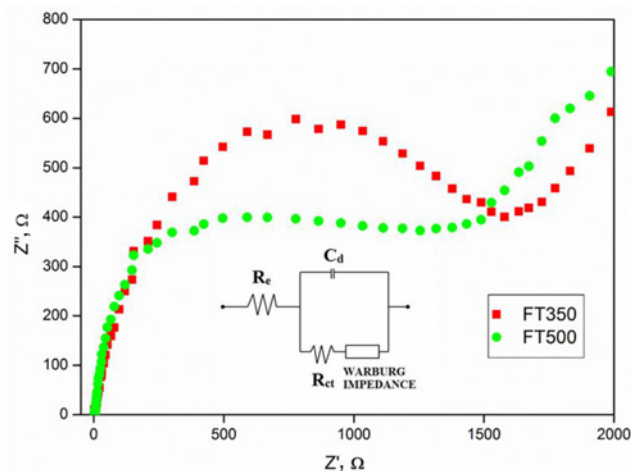


Fig. 6 EIS curve and small equivalent circuit of FT350 and FT500 samples

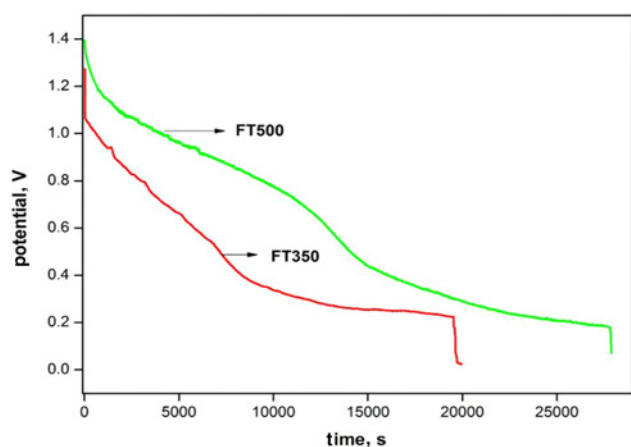


Fig. 7 Discharge curve of FT350 and FT500 samples

FT350 cell exhibits a much faster discharge transient than FT500 cell counterpart, reaching a discharge potential of 0.2 V after 2.7 h, after which the discharge voltage decreases dramatically. In contrast, FT500 cell achieves a discharge potential of 0.2 V after a discharge time of 7.7 h, after which the discharge voltage decreases dramatically. The discharge capacity of FT500 cell is 129 mA h g^{-1} whereas that of FT350 cell is 90 mA h g^{-1} . This finding indicates that FT500 sample with a high discharge capacity results in prolonged battery life compared to FT350 sample.

5. Conclusion: In summary, FeTiO_3 nanoparticles sintered at temperatures 350°C (FT350) and 500°C (FT500) were successfully prepared. The electrochemical characterisations were made to evaluate the specific capacitance and discharge behaviour for both the sintered samples. From these studies, 500°C sample as cathode material showed a better specific capacitance and discharge capacity of about 42 F g^{-1} and 129 mA h g^{-1} , respectively. The specific capacitance and discharge capacity of the sintered sample 500°C are 54 and 70% higher than those of 350°C sample. The resultant products can be eagerly applied as active materials in electrochemical energy storage applications. In addition to that the prepared FeTiO_3 nanoparticles sintered at 500°C sample can be used as cathode to be more promising for magnesium-based primary cell used in high power application.

6 References

- [1] Liu F., He H.: 'Structure–activity relationship of iron titanate catalysts in the selective catalytic reduction of NO_x with NH_3 ', *J. Phys. Chem. C*, 2010, **114**, pp. 16929–16936
- [2] Jose R., Thavasi V., Ramakrishna S.: 'Metal oxides for dye-sensitized solar cells', *J. Am. Ceram. Soc.*, 2009, **92**, pp. 289–301
- [3] Linden D., Reddy T.B.: 'Handbook of batteries' (McGraw-Hill, New York, 2002, 3rd edn.)

- [4] Li J., Xie H., Li Y.: 'Electrochemical performance of graphene oxide/polyaniline composite for supercapacitor electrode', *J. Nanosci. Nanotechnol.*, 2015, **15**, (4), pp. 3280–3283
- [5] Naoi K., Ishimoto S., Miyamoto J.-I., ET AL.: 'Second generation 'nanohybrid supercapacitor': evolution of capacitive energy storage devices', *Energy Environ. Sci.*, 2012, **5**, (11), pp. 9363–9373
- [6] Zhi M., Xiang C., Li J., ET AL.: 'Nanostructured carbon–metal oxide composite electrodes for supercapacitors: a review', *Nanoscale*, 2013, **5**, (1), pp. 72–88
- [7] Ramya R., Sivasubramanian R., Sangaranarayanan M.V.: 'Conducting polymers-based electrochemical supercapacitors—progress and prospects', *Electrochim. Acta*, 2013, **101**, pp. 109–129
- [8] Lokhande C.D., Dubal D.P., Joo O.-S.: 'Metal oxide thin film based supercapacitors', *Cur. Appl. Phys.*, 2011, **11**, (3), pp. 255–270
- [9] Zhu X., Zhu Y., Murali S., ET AL.: 'Nanostructured reduced graphene oxide/ Fe_2O_3 composite as a high-performance anode material for lithium ion batteries', *ACS Nano*, 2011, **5**, (4), pp. 3333–3338
- [10] Zhao F., Harnisch F., Schröder U., ET AL.: 'Challenges and constraints of using oxygen cathodes in microbial fuel cells', *Electrochem. Commun.*, 2006, **40**, (17), pp. 5193–5199
- [11] Wang D., Li Y., Wang Q., ET AL.: 'Nanostructured Fe_2O_3 –graphene composite as a novel electrode material for supercapacitors', *J. Solid State Electrochem.*, 2012, **16**, (6), pp. 2095–2102
- [12] Liu C., Jia Q., Yang C., ET AL.: 'Lateral flow immunochromatographic assay for sensitive pesticide detection by using Fe_3O_4 nanoparticle aggregates as color reagents', *Anal. Chem.*, 2011, **83**, (17), pp. 6778–6784
- [13] Suresh R., Vijayaraj A., Giribabu K., ET AL.: 'Fabrication of iron oxide nanoparticles: magnetic and electrochemical sensing property', *J. Mater. Sci., Mater. Electron.*, 2013, **24**, (4), pp. 1256–1263
- [14] Wang G., Zhang L., Zhang J.: 'A review of electrode materials for electrochemical supercapacitors', *Chem. Soc. Rev.*, 2012, **41**, (2), pp. 797–828
- [15] Kim Y., Gao J.B., Han S.Y., ET AL.: 'Heterojunction of FeTiO_3 nanodisc and TiO_2 nanoparticle for a novel visible light photocatalyst', *J. Phys. Chem. C*, 2009, **113**, (44), pp. 19179–19184
- [16] Tao T., Glushenkov A.M., Liu H., ET AL.: 'Ilmenite FeTiO_3 nanoflowers and their pseudocapacitance', *J. Phys. Chem. C*, 2011, **115**, (35), pp. 17297–17302
- [17] Ginley D.S., Butler M.A.: 'The photoelectrolysis of water using iron titanate anodes', *J. Appl. Phys.*, 1977, **48**, (5), pp. 2019–2021
- [18] Zhou F., Kotru S., Pandey R.K.: 'Nonlinear current–voltage characteristics of ilmenite–hematite ceramic', *Mater. Lett.*, 2003, **57**, (13–14), pp. 2104–2109
- [19] Mona J., Kale S.N., Gaikwad A.B., ET AL.: 'Chemical methods to synthesize FeTiO_3 powders', *Mater. Lett.*, 2006, **60**, (11), pp. 1425–1427
- [20] Sōmiya S., Roy R.: 'Hydrothermal synthesis of fine oxide powders', *Bull. Mater. Sci.*, 2000, **23**, (6), pp. 453–460
- [21] Gambhire A.B., Lande M.K., Rathod S.B., ET AL.: 'Synthesis and characterization of FeTiO_3 ceramics', *Arab. J. Chem.*, 2016, **9**, pp. S429–S432
- [22] Tang X., Hu K.-A.: 'The formation of ilmenite FeTiO_3 powders by a novel liquid mix and $\text{H}_2/\text{H}_2\text{O}$ reduction process', *J. Mater. Sci.*, 2006, **41**, (23), pp. 8025–8028
- [23] Raghavender A.T., Hoa Hong N., Joon Lee K., ET AL.: 'Nano-ilmenite FeTiO_3 : synthesis and characterization', *J. Magn. Magn. Mater.*, 2013, **331**, pp. 129–132
- [24] Tao T., Glushenkov A.M., Rahman M.M., ET AL.: 'Electrochimica electrochemical reactivity of ilmenite FeTiO_3 , its nanostructures and oxide-carbon nanocomposites with lithium', *Electrochim. Acta*, 2013, **108**, pp. 127–134